

11-2014

Excitation of nightside magnetosonic waves observed by Van Allen Probes

Qinghua Zhou
Changsha University of Electric Power

Fuliang Xiao
Changsha University of Electric Power

Chang Yang
Changsha University of Electric Power

Si Liu
Changsha University of Electric Power

C A. Kletzing
University of Iowa

See next page for additional authors

Follow this and additional works at: https://scholars.unh.edu/physics_facpub

 Part of the [Physics Commons](#)

Recommended Citation

Zhou, Q., et al. (2014), Excitation of nightside magnetosonic waves observed by Van Allen Probes, *J. Geophys. Res. Space Physics*, 119, 9125–9133, doi:10.1002/2014JA020481.

This Article is brought to you for free and open access by the Physics at University of New Hampshire Scholars' Repository. It has been accepted for inclusion in Physics Scholarship by an authorized administrator of University of New Hampshire Scholars' Repository. For more information, please contact nicole.hentz@unh.edu.

Authors

Qinghua Zhou, Fuliang Xiao, Chang Yang, Si Liu, C A. Kletzing, W. S. Kurth, G. B. Hospodarsky, Harlan E. Spence, Geoffrey Reeves, H. O. Funsten, J. B. Blake, D. N. Baker, and J. R. Wygant

RESEARCH ARTICLE

10.1002/2014JA020481

Special Section:

New perspectives on Earth's radiation belt regions from the prime mission of the Van Allen Probes

Key Points:

- Correlated Van Allen Probe data of MS wave and proton ring
- Growth rates are peaked at the harmonics of the proton gyrofrequency
- MS waves propagate inward divergently and outward convergently

Correspondence to:

F. Xiao,
fxiao@126.com

Citation:

Zhou, Q., et al. (2014), Excitation of nightside magnetosonic waves observed by Van Allen Probes, *J. Geophys. Res. Space Physics*, 119, 9125–9133, doi:10.1002/2014JA020481.

Received 6 AUG 2014

Accepted 22 OCT 2014

Accepted article online 26 OCT 2014

Published online 27 NOV 2014

Excitation of nightside magnetosonic waves observed by Van Allen Probes

Qinghua Zhou¹, Fuliang Xiao¹, Chang Yang¹, Si Liu¹, C. A. Kletzing², W. S. Kurth², G. B. Hospodarsky², H. E. Spence³, G. D. Reeves⁴, H. O. Funsten⁵, J. B. Blake⁶, D. N. Baker⁷, and J. R. Wygant⁸

¹School of Physics and Electronic Sciences, Changsha University of Science and Technology, Changsha, China,

²Department of Physics and Astronomy, University of Iowa, Iowa City, Iowa, USA, ³Institute for the Study of Earth, Oceans, and Space, University of New Hampshire, Durham, New Hampshire, USA, ⁴Space Science and Applications Group, Los Alamos National Laboratory, Los Alamos, New Mexico, USA, ⁵ISR Division, Los Alamos National Laboratory, Los Alamos, New Mexico, USA, ⁶The Aerospace Corporation, Los Angeles, California, USA, ⁷Laboratory for Atmospheric and Space Physics, University of Colorado Boulder, Boulder, Colorado, USA, ⁸School of Physics and Astronomy, University of Minnesota, Twin Cities, Minneapolis, Minnesota, USA

Abstract During the recovery phase of the geomagnetic storm on 30–31 March 2013, Van Allen Probe A detected enhanced magnetosonic (MS) waves in a broad range of $L = 1.8$ – 4.7 and magnetic local time (MLT) = 17 – 22 h, with a frequency range ~ 10 – 100 Hz. In the meanwhile, distinct proton ring distributions with peaks at energies of ~ 10 keV, were also observed in $L = 3.2$ – 4.6 and $L = 5.0$ – 5.6 . Using a subtracted bi-Maxwellian distribution to model the observed proton ring distribution, we perform three-dimensional ray tracing to investigate the instability, propagation, and spatial distribution of MS waves. Numerical results show that nightside MS waves are produced by proton ring distribution and grow rapidly from the source location $L = 5.6$ to the location $L = 5.0$ but remain nearly stable at locations $L < 5.0$. Moreover, waves launched toward lower L shells with different initial azimuthal angles propagate across different MLT regions with divergent paths at first, then gradually turn back toward higher L shells and propagate across different MLT regions with convergent paths. The current results further reveal that MS waves are generated by a ring distribution of ~ 10 keV proton and proton ring in one region can contribute to the MS wave power in another region.

1. Introduction

Fast magnetosonic (MS) wave (also called equatorial noise) is an electromagnetic wave emission observed close to the geomagnetic equator [Russell et al., 1970; Némec et al., 2005]. Early observational studies have shown that the waves can be observed at a wide range of L shells from $L = 2$ to 8 [Perraut et al., 1982; Boardsen et al., 1992]. Recently, Zhou et al. [2014] have presented the first report of MS waves at dipolarization fronts beyond $L = 9$. MS waves are present as a series of narrow tones, spaced at multiples of the proton gyrofrequency f_{ci} up to the lower hybrid resonance frequency f_{LH} [Perraut et al., 1982]. They are nearly linearly polarized and propagate with wave vector \mathbf{k} almost perpendicular to the ambient magnetic field \mathbf{B}_0 [Russell et al., 1970]. On the basis of observations and numeric simulations, it has been proposed that MS waves are excited by a ring distribution of protons at energies of ~ 10 keV with the ring velocity exceeding the local Alfvén speed [Curtis and Wu, 1979; Boardsen et al., 1992; Horne et al., 2000; Meredith et al., 2008; Gary et al., 2010; Liu et al., 2011]. Chen et al. [2010a] have presented a global simulation of the MS wave instability in the storm time magnetosphere. Their simulation result shows that the MS wave instability occurs at the local Alfvén speed comparable to the proton ring velocity, and the unstable frequency band can be modulated by the ratio of the ring velocity and the local Alfvén speed. Boardsen et al. [1992] and Horne et al. [2000] have performed ray tracing to calculate the raypath and path-integrated gain of MS waves.

MS waves have attracted considerable research interest because they play an important role in the dynamics of relativistic electrons. MS waves can lead to either local electron acceleration from 10 keV up to a few MeV in the outer radiation belts because of Landau resonance [Horne et al., 2007], or nonresonant transit time scattering of outer radiation belt energetic electrons because of the equatorial spatial confinement [Bortnik and Thorne, 2010; Li et al., 2014]. A recent study shows that MS wave can generate proton aurora by efficiently scattering energetic (a few keV) protons into the loss cone [Xiao et al., 2014a]. The analysis for

proton phase space density (PSD) observed by the Los Alamos National Laboratory magnetospheric plasma analyzer during the 2001 April storm show that distinct proton rings are formed over a broad magnetic local time (MLT) range from 10 h to 22 h, and MS wave instability is present over a broad range of wave frequency from ~ 5 to $35 f_{ci}$ in this region [Chen *et al.*, 2011]. Recently, Xiao *et al.* [2012] have studied the propagation characteristics of MS waves by a three-dimensional ray tracing. They show that dayside MS waves originating from different L shells can propagate either into or out of the plasmasphere, eastward or westward over a broad region of MLT. Their results can explain the different MLT distribution of observed proton source and MS waves. Xiao *et al.* [2013] have reported correlated observations of MS waves and distinct proton ring distributions collected by Cluster satellite and performed the corresponding calculation of the MS wave instability. However, they have assumed the same proton distribution everywhere from the source locations to the observed location due to lack of the simultaneous data. Furthermore, based on our knowledge, how propagation characteristics affect the spatial distribution of MS waves has seldom been reported so far.

The launching of Van Allen probes have led to the latest findings of the radiation belt electron dynamics, which include the reconfirmation of electron phase space density peak associated with local accelerations [Reeves *et al.*, 2013], the discovery of a new relativistic electron ring [Baker *et al.*, 2013] and together with the corresponding explanations [Thorne *et al.*, 2013a; Shprits *et al.*, 2013], and the identification of efficient chorus-driven acceleration of the radiation belt electrons [Thorne *et al.*, 2013b; Xiao *et al.*, 2014b]. In this study, we shall present simultaneous observations of nightside MS waves and proton rings collected by detectors onboard the Van Allen Probe A and perform a MS wave instability analysis based on the proton ring distribution at different L shells. Moreover, we shall in detail study how propagation characteristics affect the spatial distribution of MS waves.

2. Observation

The Electric and Magnetic Field Instrument Suite and Integrated Science (EMFISIS) instrumentation suite onboard the Van Allen Probes uses a triaxial fluxgate magnetometer, a triaxial magnetic search coil magnetometer, and the signals from the Electric Fields and Waves experiment to measure the background magnetic fields and a comprehensive set of wave electric and magnetic fields. The High Frequency Receiver (HFR) of EMFISIS is designed to provide spectral information from 10 kHz to 400 kHz. The Waveform Receiver (WFR) measures all six components of the electromagnetic waves in the frequency range from ~ 10 Hz up to 12 kHz and provides spectral matrices by applying the fast Fourier transform method to the autocorrelations and cross correlations of the components. The spectral matrices can be used to investigate the power spectral densities and the propagation characteristics of waves [Kletzing *et al.*, 2013].

The observations were made by Probe A during 30–31 March 2013, the recovery phase of a moderate magnetic storm with a minimum $Dst = -60$ nT (Figure 1a). Figure 1b shows the electric field spectral density in the HFR channel from 21:40 on 30 March to 00:20 UT on 31 March. During this period, Probe A moved from deep inside the plasmasphere to the outside of the plasmopause. The plasmopause crossing occurred at $L \approx 4.9$ at $\sim 23:35$ UT, as indicated in Figure 1b by the rapid drop in the upper hybrid line. Figures 1c and 1d show the magnetic and electric field spectral density in the WFR channel, respectively. Intense electromagnetic waves are observed over a broad range of $L = 1.8$ – 4.7 and $MLT = 17$ – 22 h, with wave frequencies from ~ 10 Hz to ~ 100 Hz. We use the magnetometer_uvw data from EMFISIS to define the field-aligned coordinate (FAC) system and build the UVW-FAC transformation matrix. Then we transform the spectral matrices from the UVW scientific coordinate system [Kletzing *et al.*, 2013] into the FAC system and determine the wave vector direction and wave polarization properties by the singular value decomposition (SVD) method [Santolik *et al.*, 2003]. We have checked the same data as those in the previous studies [Li *et al.*, 2013; Paulson *et al.*, 2014] and found that our results using the SVD method are consistent with theirs. Figures 1e and 1f show the wave normal angle θ and ellipticity (the ratio of the two axes of the polarization ellipse), respectively. It is indicated that the intense waves between ~ 10 Hz and ~ 100 Hz are magnetosonic waves, because they propagate at $\theta \approx 89^\circ$ and are nearly linearly polarized (ellipticity ≈ 0). MS waves are relatively weak at the region where $L < 3$ and are considerably enhanced at the larger L shell region. By using the differential fluxes data recorded by the Helium, Oxygen, Proton, and Electron (HOPE) Mass Spectrometer onboard Probe A, we derive the PSD of protons (12 eV–52 keV) for the pitch angle $\alpha = 90^\circ$. As shown in

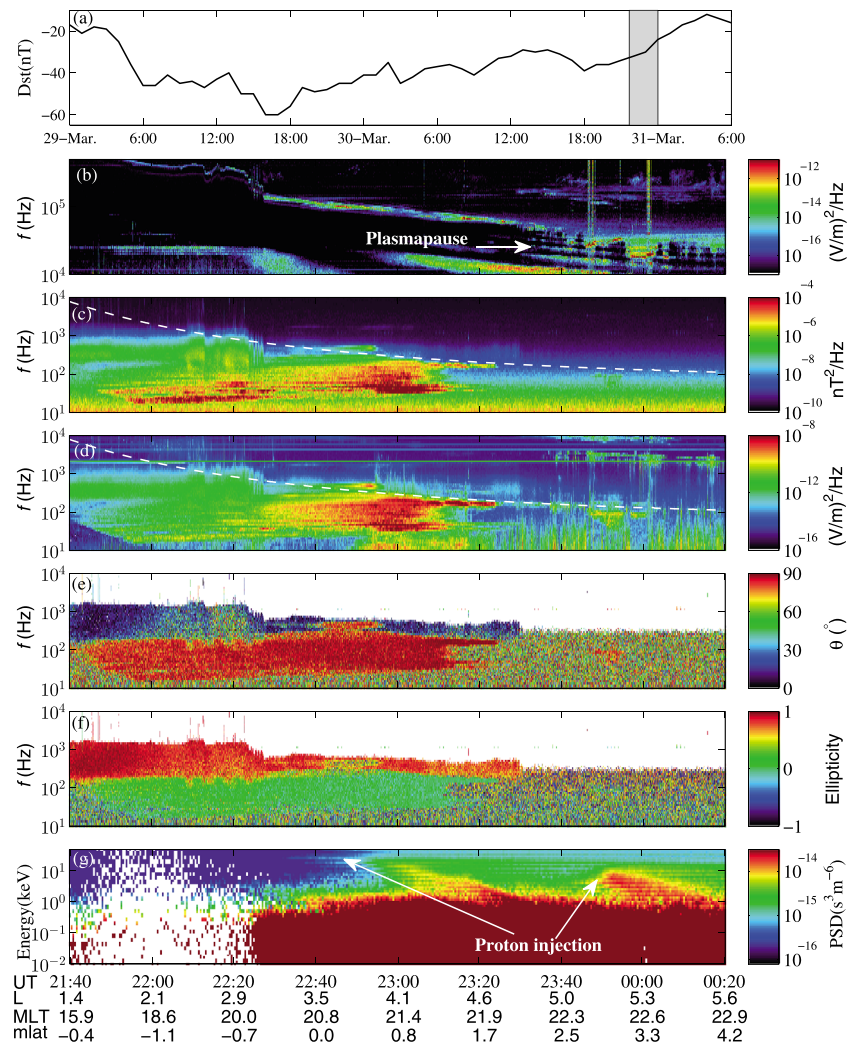


Figure 1. (a) The *Dst* index. The gray region indicates the period of the correlated data of wave and proton. (b) The electric field spectral density in the HFR channel, (c) the magnetic, and (d) electric field spectral density in the WFR channel, (e) wave normal angle, (f) ellipticity, and (g) proton PSD for the pitch angle 90° observed by Van Allen Probe A during 30–31 March 2013. The dashed lines in Figures 1c and 1d represent the local lower hybrid resonance frequency.

Figure 1g, two proton injection events were observed between 22:30 on 30 March and 00:20 UT on 31 March in an inner region ($L = 3.2\text{--}4.6$) and an outer region ($L = 5.0\text{--}5.6$).

The discrete plus symbols in Figures 2a–2d and 2e–2h represent the PSD of protons at pitch angle 90° measured at the inner region and the outer region, respectively. Distinct ring distributions are developed because of the injection events. The energy of the PSD peak is called the ring energy E_R . In the inner injection region, E_R varies from ~30 keV to ~15 keV as L increases from 3.2 to 4.6. In the outer injection region, E_R changes from ~20 keV to ~7 keV as L increases from 5.0 to 5.6.

3. Numerical Simulation

A sum of four subtracted bi-Maxwellian component is used to represent the proton ring distribution:

$$f(v_{\parallel}, v_{\perp}) = \sum_{i=1}^4 f_i(v_{\parallel}, v_{\perp}) \tag{1}$$

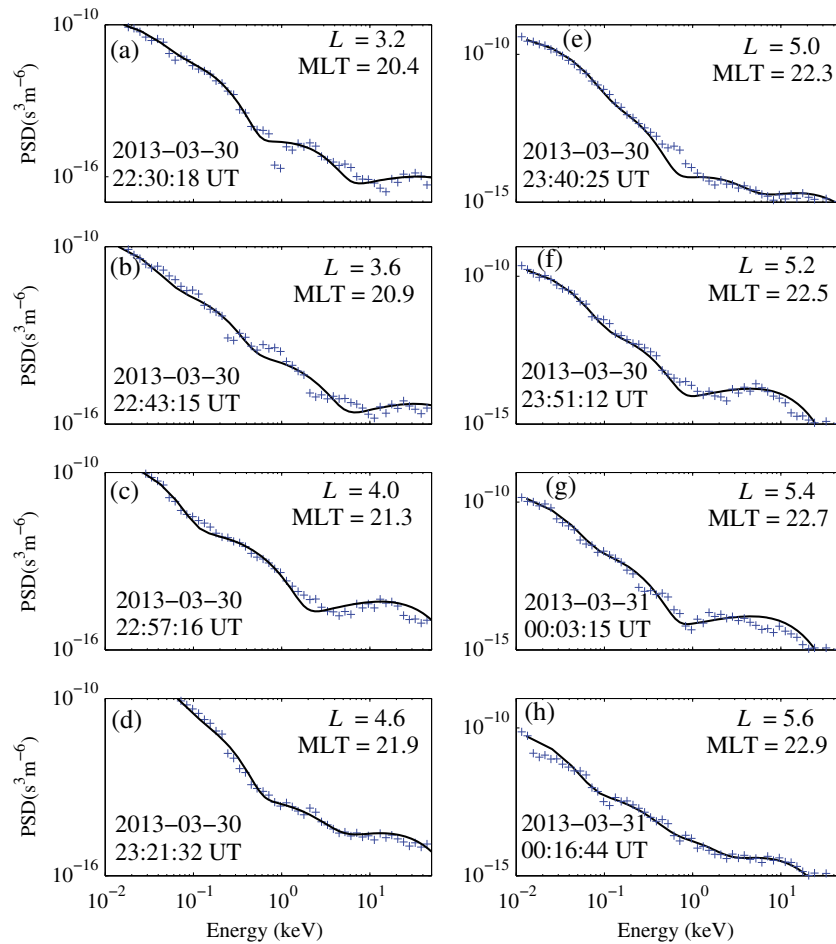


Figure 2. (a–h) Modeled subtracted Maxwellian distribution (solid) to the observed proton PSD (plus) for the pitch angle $\alpha = 90^\circ$ measured by HOPE onboard Van Allen Probe A at different L shells.

The distribution function for each species i is

$$f_i(v_{\parallel}, v_{\perp}) = \frac{N_i}{\pi^{3/2} \theta_{\perp i}^2 \theta_{\parallel i}} \exp\left(-\frac{v_{\parallel}^2}{\theta_{\parallel i}^2}\right) \left[\Delta_i \exp\left(-\frac{v_{\perp}^2}{\theta_{\perp i}^2}\right) + \frac{(1 - \Delta_i)}{(1 - \beta_i)} \left(\exp\left(-\frac{v_{\perp}^2}{\theta_{\perp i}^2}\right) - \exp\left(-\frac{v_{\perp}^2}{\beta_i \theta_{\perp i}^2}\right) \right) \right] \quad (2)$$

where N_i is the density, Δ_i and β_i are used to represent the loss cone feature of the ring distribution, and $\theta_{\parallel i}$ and $\theta_{\perp i}$ are the thermal velocities parallel and perpendicular to the background magnetic field, respectively. These parameters are obtained by performing the nonlinear least squares fitting [Marquardt, 1963; Moré, 1978] to the observed PSD. The solid lines in Figure 2 represent the distribution functions along the v_{\perp} axis ($f(v_{\parallel} = 0, v_{\perp})$).

The fitting functions are used to calculate the local growth rate of MS waves following the method introduced by Kennel [1966] and Chen *et al.* [2010b]. Figure 3 plots the scaled local growth rate of waves corresponding to those proton ring distributions in Figure 2. In the simulation, the MS waves are assumed to propagate at $\theta = 89.5^\circ$. The wave growth rates are peaked at $n\Omega_{ci}$ and rapidly fluctuate at relatively low frequencies ($3\Omega_{ci} \leq \omega < 20\Omega_{ci}$) but change smoothly at high frequencies ($\omega > 20\Omega_{ci}$). Furthermore, the growth rate at $L = 5.2$ – 5.6 is about 1 or 2 orders of magnitude higher than that at $L = 4.0$ – 5.0 or $L = 3.2$ – 3.6 . Therefore, the MS waves observed at $1.8 < L < 4.7$ in Figure 1 should come from those waves which are generated at $L > 5.0$ and propagate toward the Earth.

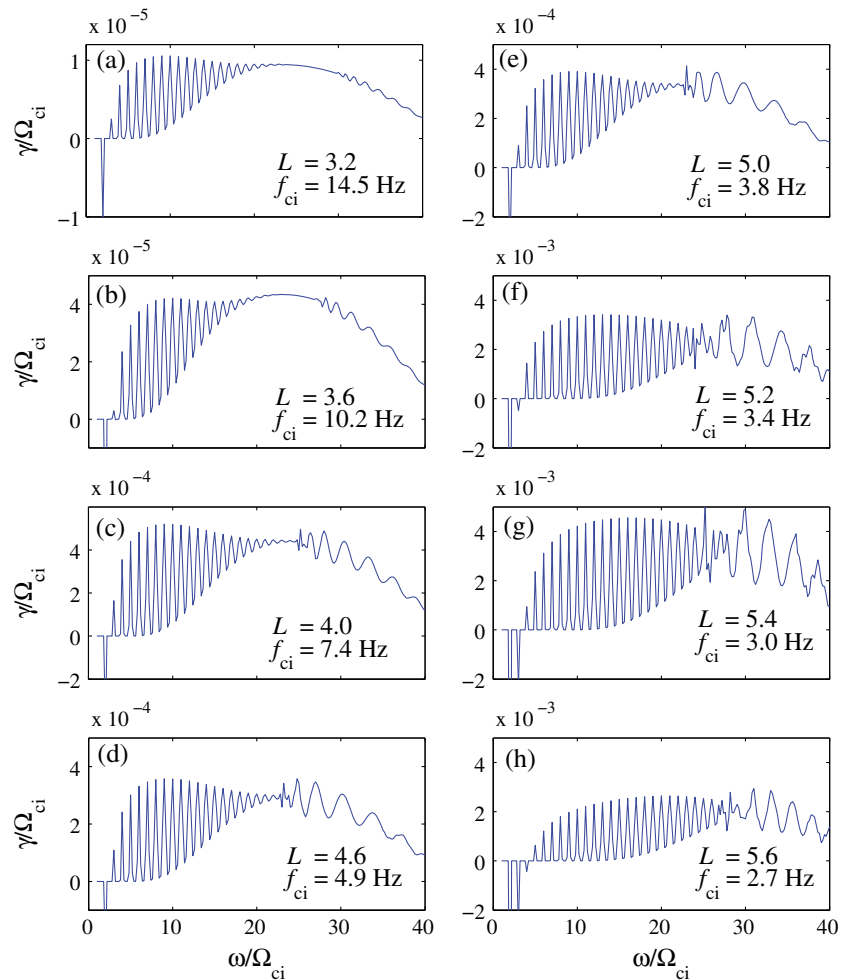


Figure 3. (a–h) Corresponding to Figure 2, simulating result of the scaled local MS wave growth rate versus the scaled wave frequency by the subtracted bi-Maxwellian distribution.

The raypath and path-integrated gain of MS waves are simulated by performing ray tracing in a three-dimensional space. The ray tracing program has been developed based on the methodology of the ray tracing program HOTRAY [Horne, 1989] and has been applied to study the excitation and propagation of electromagnetic waves in space plasmas [Xiao et al., 2012, 2013; Zhou et al., 2012, 2013]. The program determines the raypath and the wave normal angle at each time step by integrating Hamilton's equations [Suchy, 1981; Horne, 1989]. Here we adopt a dipole magnetic field model and a background electron density model which is incorporated by the global core plasma density model [Gallagher et al., 2000] and a field-aligned density model [Denton et al., 2002]. In order to perform ray tracing, we define two coordinate systems following the previous works [Horne, 1989; Chen et al., 2009]. The first system (XYZ) is the Cartesian coordinate system centering on the Earth. The Z axis is along the geomagnetic axis pointing north, the X axis is orthogonal to the Z axis and pointing away from the Sun, and the Y axis completes the right-handed set. The second system (xyz) is a local Cartesian system centered on a point p of the raypath. As shown in Figure 4a, the z axis is along the local magnetic field direction, the x axis is orthogonal to the z axis and lies in the meridian plane pointing away from the Earth at the equator, and the y axis completes the right-handed set. Between the wave vector \mathbf{k} and the z axis θ is the wave normal angle, and η is the azimuthal angle between the projection of \mathbf{k} onto the xy plane and the x axis.

We fit the observed PSD of protons by the bi-Maxwellian distribution in the region $L = 1.4$ – 5.6 at 0.1 spacing and assume the same distribution at the same L shell. The local growth rate γ can be evaluated by using the

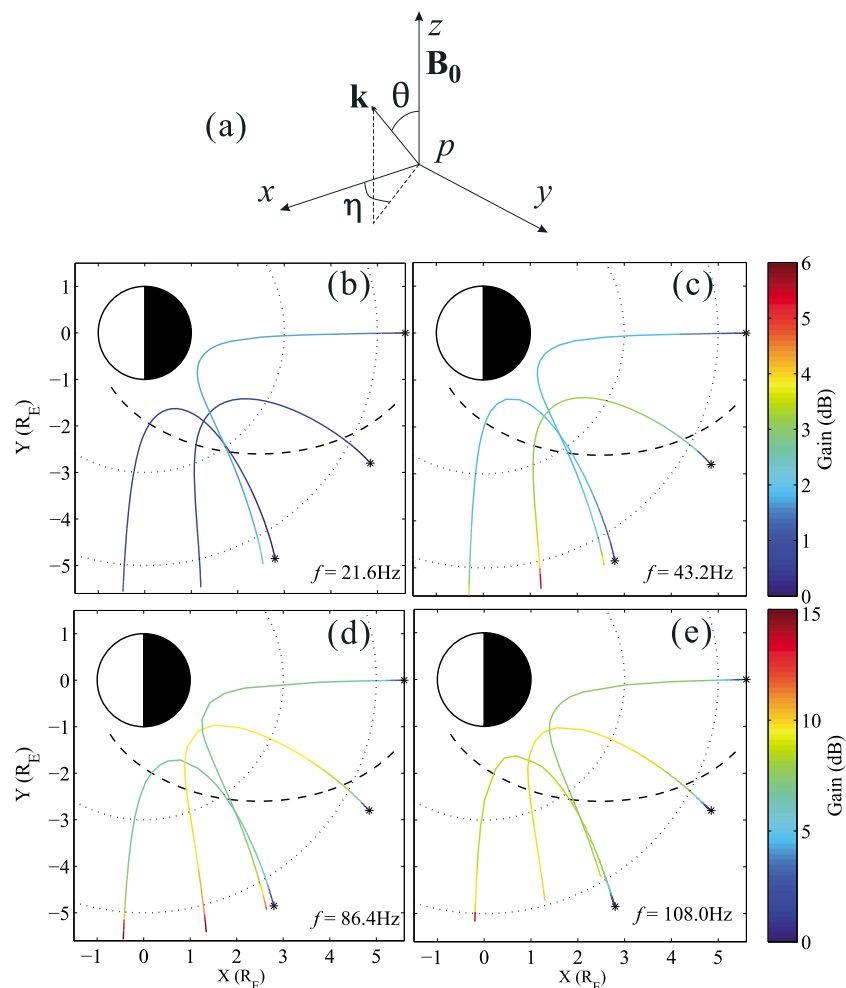


Figure 4. (a) Geometry of wave vector \mathbf{k} in a local Cartesian system centered on a point p of the raypath in ray tracing. (b–e) The projections of raypaths on the X - Y plane. The waves start at the locations (stars): $L = 5.6$, MLT = 20 h, 22 h, and 24 h, with $\theta_0 = 89.5^\circ$ and different wave frequencies. Path-integrated gain of the waves is color coded along the raypath. The dashed line indicates Van Allen Probe A orbital trajectory from 21:40 UT on 30 March to 00:20 UT on 31 March. The concentric dotted arcs indicate the locations $L = 3$ and 5 , respectively.

fitting function at each step during ray tracing. The path-integrated wave gain in decibel is calculated by integrating γ along the raypath:

$$\text{Gain} = 20 \log_{10} \left(\exp \left(\int \gamma dt \right) \right) \quad (3)$$

Figures 4b–4e show simulating results of raypaths and path-integrated gain (color coded). The MS waves launched at equatorial location $L = 5.6$, MLT = 20 h, 22 h, and 24 h, with initial wave normal angle $\theta_0 = 89.5^\circ$ and different wave frequencies $f = 21.6 \text{ Hz}$ ($\sim 8f_{ci}$), 43.2 Hz ($\sim 16f_{ci}$), 86.4 Hz ($\sim 32f_{ci}$), and 108.0 Hz ($\sim 40f_{ci}$). These waves propagate toward lower L shell at first and then gradually turn back toward high L shells due to approaching the higher-density region [Xiao *et al.*, 2012]. All the rays pass through the observed region. Wave gain increases rapidly outside the region $L = 5.0$ but remains nearly constant in the region $L < 5.0$, consistent with the simulation results of local growth rate in Figure 3 and the previous work [Horne *et al.*, 2000].

MS waves can propagate both radially and azimuthally, so the MS waves observed at any specified location are the superposition of a series of MS waves generated in a broad source region. Figure 5 shows the raypaths of the MS waves launched at the same location as that in Figure 4, with $\theta_0 = 89.5^\circ$, $f = 43.2 \text{ Hz}$ ($\sim 16f_{ci}$), and 86.4 Hz ($\sim 32f_{ci}$). The initial azimuthal angles cover from 161° to 199° at 2° spacing are indicated by the color lines. All the waves propagate toward lower L shells with divergent raypaths at first then

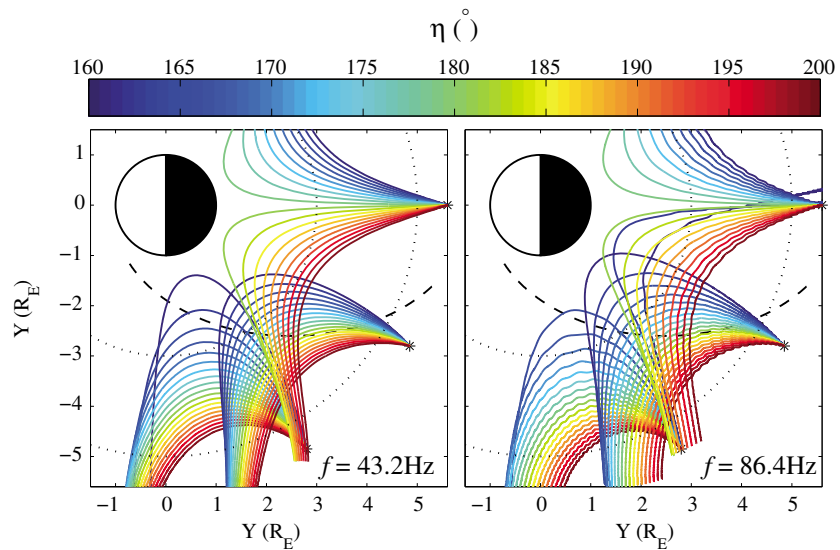


Figure 5. The projections of raypaths of the MS waves for $\theta_0 = 89.5^\circ$ and different initial azimuthal angles η_0 . The concentric dotted arcs indicate the locations $L = 3$ and 5 , respectively. The asterisks denote the source locations: $L = 5.6$, $\text{MLT} = 20$ h, 22 h, and 24 h.

gradually turn back toward higher L shells with convergent raypaths when they approach higher-density region. The waves launched at $\text{MLT} = 24$ h propagate eastward (later MLT) for $\eta_0 < 180^\circ$ and westward (earlier MLT) for $\eta_0 > 180^\circ$. Almost all the waves launched at $\text{MLT} = 20$ h and 22 h propagate westward (earlier MLT), except for $\text{MLT} = 20$ h, $f = 86.4$ Hz, $\eta_0 = 161^\circ$, and 163° . Only few raypaths can penetrate into the near-Earth region (e.g., $L < 3$) from a remote source region, consistent with the observation (Figure 1).

4. Summary

An event of nightside magnetosonic waves observed by the EMFISIS instrument on the Van Allen Probe A during the recovery phase of the geomagnetic storm on 30 March 2013 are presented. Proton PSD at 90° pitch angle measured by HOPE is fitted with a sum of subtracted bi-Maxwellian components to model the ring distribution and the fitting functions are used to calculate the local growth rate of MS waves at different L shells. Then three-dimensional ray tracing is performed to studying how propagation characteristics affect the spatial distribution of MS waves in detail. The main results of this paper can be summarized as follows:

1. Intense MS waves are observed over a broad range of $L = 1.8\text{--}4.7$ and $\text{MLT} = 17\text{--}22$ h, with wave frequencies from ~ 10 Hz to ~ 100 Hz. Simultaneous observations of PSD show that the distinct proton ring is present in $L = 3.2\text{--}4.6$ and $L = 5.0\text{--}5.6$, which provides the source of free energy for the excitation of MS waves.
2. The wave growth rates are peaked at $n\Omega_{ci}$ and rapidly fluctuate at relatively low frequencies ($3\Omega_{ci} \leq \omega < 20\Omega_{ci}$) but change smoothly at high frequencies ($\omega > 20\Omega_{ci}$). The growth rate at $L = 5.2\text{--}5.6$ is about 1 or 2 orders of magnitude higher than that at $L = 4.0\text{--}5.0$ or $L = 3.2\text{--}3.6$, suggesting that the source waves of the observed MS waves should occur at $L > 5.0$ and propagate toward the Earth. This indicates that proton ring in one region can contribute to the MS wave power in another region.
3. The nightside MS waves launched at the equatorial location $L = 5.6$ grow rapidly at the outside of $L = 5.0$ but remain nearly stable in $L < 5.0$. The waves propagate toward lower L shells with divergent raypaths at first then gradually turn back toward higher L shells with convergent raypaths. The combination of the path-integrated gain pattern and the propagation characteristics perhaps explain the spatial distribution characteristics that the observed MS wave power is relatively weak in the near-Earth region ($L < 3$) and becomes much stronger in the region far from the Earth ($L > 3$).

Acknowledgments

This work is supported by 973 Program 2012CB825603, the National Natural Science Foundation of China grants 41204114 and 41274165, the Aid Program for Science and Technology Innovative Research Team in Higher Educational Institutions of Hunan Province, and the Construct Program of the Key Discipline in Hunan Province. All the Van Allen Probes data are publicly available at <https://emfisis.physics.uiowa.edu/data/index> by the EMFISIS instrument and at http://www.rbbsp-ect.lanl.gov/data_pub/ by the HOPE instrument. This work was also supported from JHU/APL contracts 921647 and 967399 under NASA Prime contract NASS-01072.

Yuming Wang thanks the reviewers for their assistance in evaluating the paper.

References

- Baker, D. N., et al. (2013), A long-lived relativistic electron storage ring embedded in Earth's outer Van Allen belt, *Science*, *340*(6129), 186–190, doi:10.1126/science.1233518.
- Boardsen, S. A., D. L. Gallagher, D. A. Gurnett, W. K. Peterson, and J. L. Green (1992), Funnel-shaped, low-frequency equatorial waves, *J. Geophys. Res.*, *97*, 14,967–14,976, doi:10.1029/92JA00827.
- Bortnik, J., and R. M. Thorne (2010), Transit time scattering of energetic electrons due to equatorially confined magnetosonic waves, *J. Geophys. Res.*, *115*, A07213, doi:10.1029/2010JA015283.
- Chen, L., J. Bortnik, R. M. Thorne, R. Horne, and V. K. Jordanova (2009), Three-dimensional ray tracing of VLF waves in a magnetospheric environment containing a plasmaspheric plume, *Geophys. Res. Lett.*, *36*, L22101, doi:10.1029/2009GL040451.
- Chen, L., R. M. Thorne, V. K. Jordanova, and R. B. Horne (2010a), Global simulation of magnetosonic waves instability in the storm time magnetosphere, *J. Geophys. Res.*, *115*, A11222, doi:10.1029/2010JA015707.
- Chen, L., R. M. Thorne, V. K. Jordanova, C.-P. Wang, M. Gkioulidou, L. Lyons, and R. B. Horne (2010b), Global simulation of EMIC wave excitation during the 21 April 2001 storm from coupled RCM-RAM-HOTRAY modeling, *J. Geophys. Res.*, *115*, A07209, doi:10.1029/2009JA015075.
- Chen, L., R. M. Thorne, V. K. Jordanova, M. F. Thomsen, and R. B. Horne (2011), Magnetosonic wave instability analysis for proton ring distributions observed by the LANL magnetospheric plasma analyzer, *J. Geophys. Res.*, *116*, A03223, doi:10.1029/2010JA016068.
- Curtis, S. A., and C. S. Wu (1979), Gyroharmonic emissions induced by energetic ions in the equatorial plasmasphere, *J. Geophys. Res.*, *84*, 2597–2607, doi:10.1029/JA084iA06p02597.
- Denton, R. E., J. Goldstein, J. D. Menietti, and S. L. Young (2002), Magnetospheric electron density model inferred from polar plasma wave data, *J. Geophys. Res.*, *107*(A11), 1386, doi:10.1029/2001JA009136.
- Gallagher, D. L., P. D. Craven, and R. H. Comfort (2000), Global core plasma model, *J. Geophys. Res.*, *105*, 18,819–18,833.
- Gary, S. P., K. Liu, D. Winske, and R. E. Denton (2010), Ion Bernstein instability in the terrestrial magnetosphere: Linear dispersion theory, *J. Geophys. Res.*, *115*, A12209, doi:10.1029/2010JA015965.
- Horne, R. B. (1989), Path-integrated growth of electrostatic waves: The generation of terrestrial myriametric radiation, *J. Geophys. Res.*, *94*, 8895–8909.
- Horne, R. B., G. V. Wheeler, and H. S. C. K. Alleyne (2000), Proton and electron heating by radially propagating fast magnetosonic waves, *J. Geophys. Res.*, *105*(A12), 27,597–27,610, doi:10.1029/2000JA000018.
- Horne, R. B., R. M. Thorne, S. A. Glauert, N. P. Meredith, D. Pokhotelov, and O. Santolík (2007), Electron acceleration in the Van Allen radiation belts by fast magnetosonic waves, *Geophys. Res. Lett.*, *34*, L17107, doi:10.1029/2007GL030267.
- Kennel, C. (1966), Low-frequency whistler mode, *Phys. Fluids*, *9*, 2190–2202.
- Kletzing, C. A., et al. (2013), The Electric and Magnetic Field Instrument Suite and Integrated Science (EMFISIS) on RBSP, *Space Sci. Rev.*, *179*, 127–181, doi:10.1007/s11214-013-9993-6.
- Li, J., et al. (2014), Interactions between magnetosonic waves and radiation belt electrons: Comparisons of quasi-linear calculations with test particle simulations, *Geophys. Res. Lett.*, *41*, 4828–4834, doi:10.1002/2014GL060461.
- Li, W., et al. (2013), An unusual enhancement of low-frequency plasmaspheric hiss in the outer plasmasphere associated with substorm-injected electrons, *Geophys. Res. Lett.*, *40*, 3798–3803, doi:10.1002/grl.50787.
- Liu, K., S. P. Gary, and D. Winske (2011), Excitation of magnetosonic waves in the terrestrial magnetosphere: Particle-in-cell simulations, *J. Geophys. Res.*, *116*, A07212, doi:10.1029/2010JA016372.
- Marquardt, D. W. (1963), An algorithm for least-squares estimation of nonlinear parameters, *J. Soc. Ind. Appl. Math.*, *11*(2), 431–441.
- Meredith, N. P., R. B. Horne, and R. R. Anderson (2008), Survey of magnetosonic waves and proton ring distributions in the Earth's inner magnetosphere, *J. Geophys. Res.*, *113*, A06213, doi:10.1029/2007JA012975.
- More, J. J. (1978), The levenberg-marquardt algorithm: Implementation and theory, *Lect. Notes Math.*, *630*, 105–116, doi:10.1007/BFb0067700.
- Němec, F., O. Santolík, K. Gereová, E. Macušová, Y. de Conchy, and N. Cornilleau-Wehrlin (2005), Initial results of a survey of equatorial noise emissions observed by the Cluster spacecraft, *Planet. Space Sci.*, *53*, 291–298, doi:10.1016/j.pss.2004.09.055.
- Paulson, K. W., C. W. Smith, M. R. Lessard, M. J. Engebretson, R. B. Torbert, and C. A. Kletzing (2014), In situ observations of Pc1 pearl pulsations by the Van Allen Probes, *Geophys. Res. Lett.*, *41*, 1823–1829, doi:10.1002/2013GL059187.
- Perraut, S., A. Roux, P. Robert, R. Gendrin, J. Sauvaud, J. Bosqued, G. Kremser, and A. Korth (1982), A systematic study of ULF waves above $F_{\mu+}$ from GEOS 1 and 2 measurements and their relationships with proton ring distributions, *J. Geophys. Res.*, *87*(A1), 6219–6236, doi:10.1029/JA087iA08p06219.
- Reeves, G. D., et al. (2013), Electron acceleration in the heart of the Van Allen radiation belts, *Science*, *341*(6149), 991–994, doi:10.1126/science.1237743.
- Russell, C. T., R. E. Holzer, and E. J. Smith (1970),OGO 3 observations of ELF noise in the magnetosphere: 2. The nature of the equatorial noise, *J. Geophys. Res.*, *75*(4), 755–768, doi:10.1029/JA075i004p00755.
- Santolík, O., M. Parrot, and F. Lefeuvre (2003), Singular value decomposition methods for wave propagation analysis, *Radio Sci.*, *38*(1), 1010, doi:10.1029/2000RS002523.
- Shprits, Y. Y., D. Subbotin, A. Drozdov, M. E. Usanova, A. Kellerman, K. Orlova, D. N. Baker, D. L. Turner, and K.-C. Kim (2013), Unusual stable trapping of the ultrarelativistic electrons in the Van Allen radiation belts, *Nat. Phys.*, *9*, 699–703, doi:10.1038/nphys2760.
- Suchy, K. (1981), Real Hamilton equations of geomagnetic optics for media with moderate absorption, *Radio Sci.*, *16*, 1179–1182.
- Thorne, R. M., et al. (2013a), Evolution and slow decay of an unusual narrow ring of relativistic electrons near $L \sim 3.2$ following the September 2012 magnetic storm, *Geophys. Res. Lett.*, *40*, 3507–3511, doi:10.1002/grl.50627.
- Thorne, R. M., et al. (2013b), Rapid local acceleration of relativistic radiation-belt electrons by magnetospheric chorus, *Nature*, *504*, 411–414, doi:10.1038/nature12889.
- Xiao, F., Q. Zhou, Z. He, and L. Tang (2012), Three-dimensional ray tracing of fast magnetosonic waves, *J. Geophys. Res.*, *117*, A06208, doi:10.1029/2012JA017589.
- Xiao, F., Q. Zhou, Z. He, C. Yang, Y. He, and L. Tang (2013), Magnetosonic wave instability by proton ring distributions: Simultaneous data and modeling, *J. Geophys. Res. Space Physics*, *118*, 4053–4058, doi:10.1002/jgra.50401.
- Xiao, F., Q. Zong, Y. Wang, Z. He, Z. Su, C. Yang, and Q. Zhou (2014a), Generation of proton aurora by magnetosonic waves, *Sci. Rep.*, *4*, 5190, doi:10.1038/srep05190.
- Xiao, F., et al. (2014b), Chorus acceleration of radiation belt relativistic electrons during March 2013 geomagnetic storm, *J. Geophys. Res. Space Physics*, *119*, 3325–3332, doi:10.1002/2014JA019822.
- Zhou, M., B. Ni, S. Huang, X. Deng, M. Ashour-Abdalla, Y. Nishimura, Z. Yuan, Y. Pang, and H. Li (2014), Observation of large-amplitude magnetosonic waves at dipolarization fronts, *J. Geophys. Res. Space Physics*, *119*, 4335–4347, doi:10.1002/2014JA019796.

Zhou, Q., F. Xiao, J. Shi, and L. Tang (2012), Instability and propagation of EMIC waves in the magnetosphere by a kappa distribution, *J. Geophys. Res.*, *117*, A06203, doi:10.1029/2011JA017296.

Zhou, Q., F. Xiao, J. Shi, C. Yang, Y. He, and L. Tang (2013), Excitation of electromagnetic ion cyclotron waves under different geomagnetic activities: THEMIS observation and modeling, *J. Geophys. Res. Space Physics*, *118*, 340–349, doi:10.1029/2012JA018325.